Journal of Molecular Catalysis A: Chemical 349 (2011) 20–27

Contents lists available at SciVerse ScienceDirect

Journal of Molecular Catalysis A: Chemical

journal homepage: www.elsevier.com/locate/molcata

Characterization of coupled NiO/TiO_2 photocatalyst for the photocatalytic reduction of Cr(VI) in aqueous solution

Young Ku*, Chia-Nan Lin, Wei-Ming Hou

Department of Chemical Engineering, National Taiwan University of Science and Technology, 43, Keelung Road, Section 4, Taipei 106, Taiwan

ARTICLE INFO

Article history:
Received 27 March 2011
Received in revised form 29 June 2011
Accepted 15 August 2011
Available online 22 August 2011

Keywords:
NiO/TiO_2
p–n junction
Photocatalytic reduction
Hexavalent chromium
Sol–gel

ABSTRACT

NiO/TiO_2 coupled photocatalysts were fabricated by sol–gel process in this study. The coupled catalyst exhibited higher response of surface photovoltage than pure TiO_2 indicating that the recombination of photogenerated electron–hole pairs was retarded by the inner electric field caused by p–n junction region. Photocatalytic reduction of hexavalent chromium in aqueous solution was studied using these NiO/TiO_2 coupled photocatalysts prepared with various NiO loadings and calcined temperatures. The coupling of NiO strongly affects the performance of coupled photocatalysts, including the retard of phase transformation of TiO_2, the decrement of particle size and the enhancement of separation efficiency of photogenerated electron–hole pairs. The addition of ethanol as a sacrificial agent significantly increased the photocatalytic activity of hexavalent chromium reduction using these NiO/TiO_2 coupled photocatalysts.

1. Introduction

Titanium dioxide (TiO_2) has been used for a wide range of photocatalytic applications including solar energy conversion, hydrogen evolution, and detoxification of refractory compounds, because of its relatively high photocatalytic activity, non-toxic nature and stability [1,2]. The reduction of heavy metal in aqueous solution by photocatalytic process using semiconductors is a relatively new and effective technology. Ku and Jung [3] revealed that hexavalent chromium, Cr(VI), was efficiently reduced by UV/TiO_2 process in acidic solutions containing 0.5% ethanol as scavenger for holes. Chakrabarti et al. [4] investigated the Cr(VI) reduction in aqueous solution using ZnO as photocatalyst and reported that 90% Cr(VI) was reduced with appropriate operational conditions. However, the rapid recombination of photogenerated electron–hole pairs decreases the photo quantum efficiency of photocatalytic processes. Therefore, many studies have been devoted to the efficiency improvement of photocatalysts [5–7].

The p–n junction is formed in the interface as a space charge region when p-type (hole-rich) and n-type (electron-rich) semiconductors are contacted. The electron and hole carriers are diffused to p-type and n-type semiconductor, respectively. The inner electric field is established at the equilibrium of electron and hole diffusions, and then acts as a potential barrier to prevent the combination of electron and hole. The potential of electric field permits for the movement of free electrons from p-type to n-type semiconductors and the movement of free holes from n-type to p-type semiconductors. Therefore, the photogenerated electron–hole pairs excited by UV irradiation are efficiently separated by the inner electric field to minimize the recombination.

Recently, several p–n junction photocatalysts have been investigated because the photogenerated electrons and holes were effectively separated to increase the quantum yields of photocatalytic reactions. NiO is a p-type semiconductor frequently used as a cocatalyst loaded with different photocatalysts because the loading process is simple and inexpensive, and the photocatalysts loaded with NiO exhibited higher efficiencies for photocatalytic water splitting [8–10]. Sreethawong et al. [11] prepared the mesoporous NiO/TiO_2 using sol–gel process combined with template, and indicated the prepared NiO/TiO_2 demonstrated higher photocatalytic activities for H_2 evolution from aqueous methanol solutions. Chen et al. [5] prepared p-type ZnO by thermal decomposition and fabricated the p–n junction ZnO/TiO_2 photocatalyst. The application of ZnO/TiO_2 shows noticeable improvements for photocatalytic reduction of $Cr_2O_7^{2-}$ in aqueous solutions than pure TiO_2.

In this study, the p–n junction NiO/TiO_2 photocatalysts were fabricated by incorporating NiO to TiO_2 by sol–gel process. The effects of NiO dosage on the crystal and surface characterizations of NiO/TiO_2 photocatalyst were investigated, including crystal phase transformation of TiO_2 and variation of surface area. The surface photovoltage spectroscopy was utilized to verify the separation efficiency of photogenerated electron–hole pairs. The photocatalytic reduction of hexavalent chromium in aqueous solution was also studied using NiO/TiO_2 photocatalyst coupled with various NiO

* Corresponding author. Tel.: +886 2 27333141x7606; fax: +886 2 23785535.
E-mail address: ku508@mail.ntust.edu.tw (Y. Ku).

1381-1169/$ – see front matter © 2011 Elsevier B.V. All rights reserved.
doi:10.1016/j.molcata.2011.08.006

dosages. Ethanol was employed as hole scavenger during the photocatalytic process to examine the improvement of photocatalytic activity. The reaction rates were determined under various operating conditions and the rate parameters are expressed in terms of an apparent first order rate equation.

2. Experimental

The TiO_2 photocatalyst was fabricated by sol–gel process with titanium n-butoxide ($Ti(OC_4H_9)_4$, Acros) used as the precursor for TiO_2. After introducing 3.7 g of ethanol (C_2H_5OH, Acros) into 9.6 g of acetic acid (CH_3COOH, Panreac), 6.8 g of $Ti(OC_4H_9)_4$ was added to the solution and stirred vigorously for 72 h. The colloidal solution was dried at 80 °C for 2 h. The dried powders were then calcined in air for 2 h, temperature ranging from 400 to 600 °C; followed by cooling to form TiO_2 powder at room temperature. For the preparation of coupled NiO/TiO_2 photocatalysts, nickel nitrate hexahydrate ($Ni(NO_3)_2{\cdot}6H_2O$, Acros) was used as the precursor for NiO. Predetermined amount of $Ni(NO_3)_2{\cdot}6H_2O$ was added into the TiO_2 sol before stirring 72 h. The coupled NiO/TiO_2 photocatalyst was thereafter fabricated by sol–gel process described in above section. The calcined TiO_2 or NiO/TiO_2 powder was then slightly ground into fine particles prior to characterization and further applications for photocatalysis.

Thermogravimetry–differential thermal analysis (TG–DTA, *Perkin Elmer*, Diamond TG/DTA) was used to measure the thermal decomposition and crystallization of sample precursors with a heating rate of 10 °C/min in flowing air up to 800 °C. X-ray diffraction (XRD, *Philip*, X'Pert, Cu Kα radiation of λ = 1.5418 Å) was used to identify the crystallization level and crystal phase of samples, and the monochromated Cu Kα radiation was operated at 45 kV and 40 mA. Powders were examined at a range of 2θ from 20° to 80° with a sampling internal of 0.02° and scan speed 6°/min. Field Emission Scanning Electron Microscopy (FESEM, *JEOL*, JSM-6500F) was operated at 15 kV, and used to measure the surface morphology of the prepared samples. Brunauer–Emmett–Teller analyzer (BET, *Quantachrome*, Autosorb-1) was applied to determine the specific surface area of the prepared samples. UV–vis diffuse reflectance spectroscopy (UV-vis DRS, *Jasco*, ISV-469) was used to examine the band gap energy of the prepared f samples. X-ray Photoelectron Spectroscopy (XPS, *Thermo Scientific*, Theta Probe) was used to measures the elemental composition, chemical state and electronic state of the elements existed on the surface of the prepared samples. Zeta meter (*Malvern*, S2000) was used to measure surface charge and the zero point of charge (*Zpc*) of the prepared photocatalysts. Surface photovoltage (SPV) was monitored to realize the surface potential of an irradiated semiconductor while generating electron–hole pairs. The monochromatic light was emitted from an *Osram* 150 W halogen lamp filtered by a 0.25 m monochromator (*Photon Technology*). The induced SPV was measured by using a buffer circuit and a lock-in amplifier (*EG&G*, 5302).

The photocatalytic activity of the prepared NiO/TiO_2 coupled photocatalyst was evaluated by reducing potassium dichromate ($K_2Cr_2O_7$, Ferak) in aqueous solution at 24 ± 1 °C contained in an inner irradiation stirred reactor. 1 g NiO/TiO_2 was suspended in 1-L aqueous solution containing 20 mg/L $Cr_2O_7^{2-}$ ions. The initial pH of reaction solution was adjusted to desired level by additions of sodium hydroxide (NaOH, Acros) and nitric acid (HNO_3, Acros) solutions. The suspension was placed in a dark surrounding for 30 min to achieve adsorption equilibrium of $Cr_2O_7^{2-}$ ions by NiO/TiO_2. Photocatalytic reduction of $Cr_2O_7^{2-}$ ions was assumed to be started when the pre-warmed high-pressure mercury lamp (100 W, 365 nm) within the reactor was turned on. Aliquots of the suspension were sampled at each intermittent period. After filtering the samples by a 0.2 μm Millipore filter, concentration of $Cr_2O_7^{2-}$ ions in aqueous solution was measured by an UV–vis spectrometer (*Jasco*, V-550) at 349 nm.

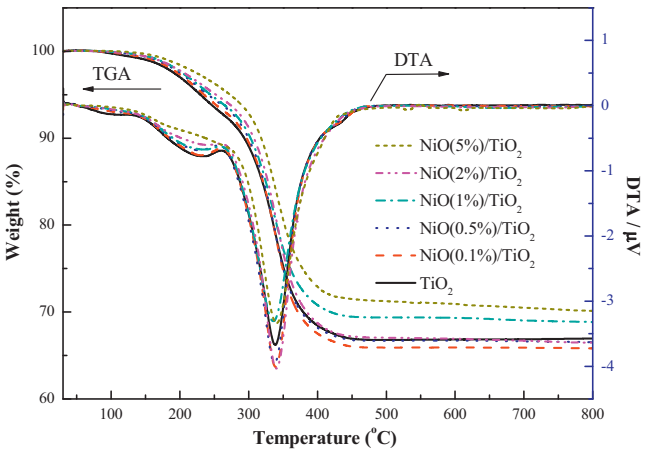

Fig. 1. TG–DTA curves of TiO_2 coupled with various dosages of NiO.

3. Results and discussion

The TGA and DTA curves of TiO_2 gel loaded with different amounts of nickel precursor sintered at temperature ranging from 30 to 800 °C are shown in Fig. 1. Minor weight losses examined within the range of 150–280 °C were attributed to the evaporation of adsorbed water and ethanol from titanium(IV) n-butoxide and residual solvent, respectively. Significant weight losses were observed between 280 and 450 °C corresponded to the major exothermic peak at 338 °C resulted from the burnout of hydroxyl groups and organics. There was no obvious weight loss in the TGA curve above 450 °C because most organics were already removed. Korošec and Bukovec [12] reported that the transformation of $NiNO_3$ into NiO was taken place from 280 to 320 °C; however, the amount of NiO was too little to be distinguished in this study.

XRD patterns of the prepared NiO(0.1%)/TiO_2 samples, calcined in the temperature range of 300–600 °C for 2 h in air atmosphere, are shown in Fig. 2. The variation of XRD patterns of the NiO(0.1%)/TiO_2 samples calcined at 300 and 400 °C indicated the phase transformation of TiO_2 from amorphous to anatase (1 0 1) structure. The increasing peak intensity of rutile (1 1 0) for samples calcined at 600 °C demonstrated the phase transformation of TiO_2

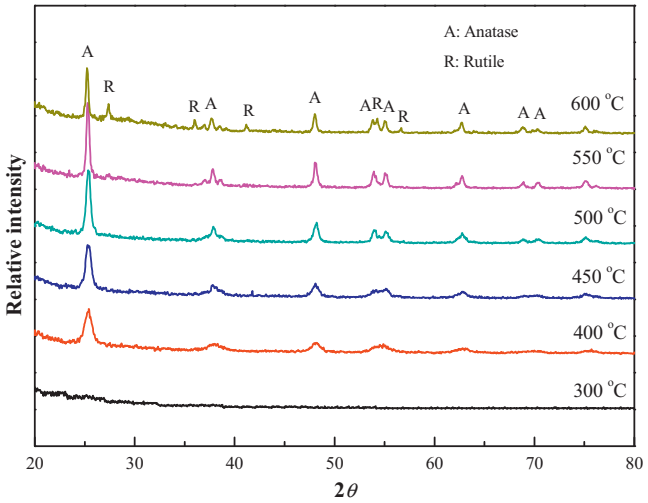

Fig. 2. XRD patterns of NiO(0.1%)/TiO_2 calcined at various temperatures.

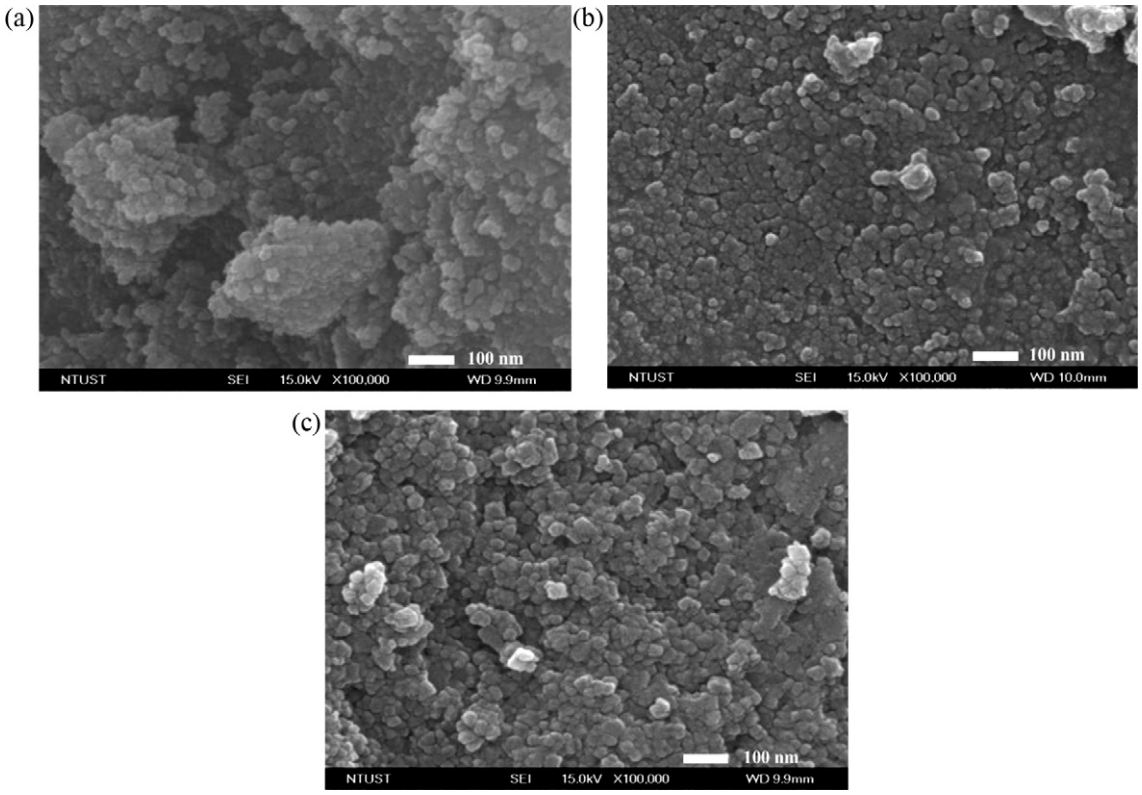

Fig. 3. SEM photographs of NiO(5%)/TiO_2 calcined at (a) 400 °C, (b) 500 °C and (c) 600 °C.

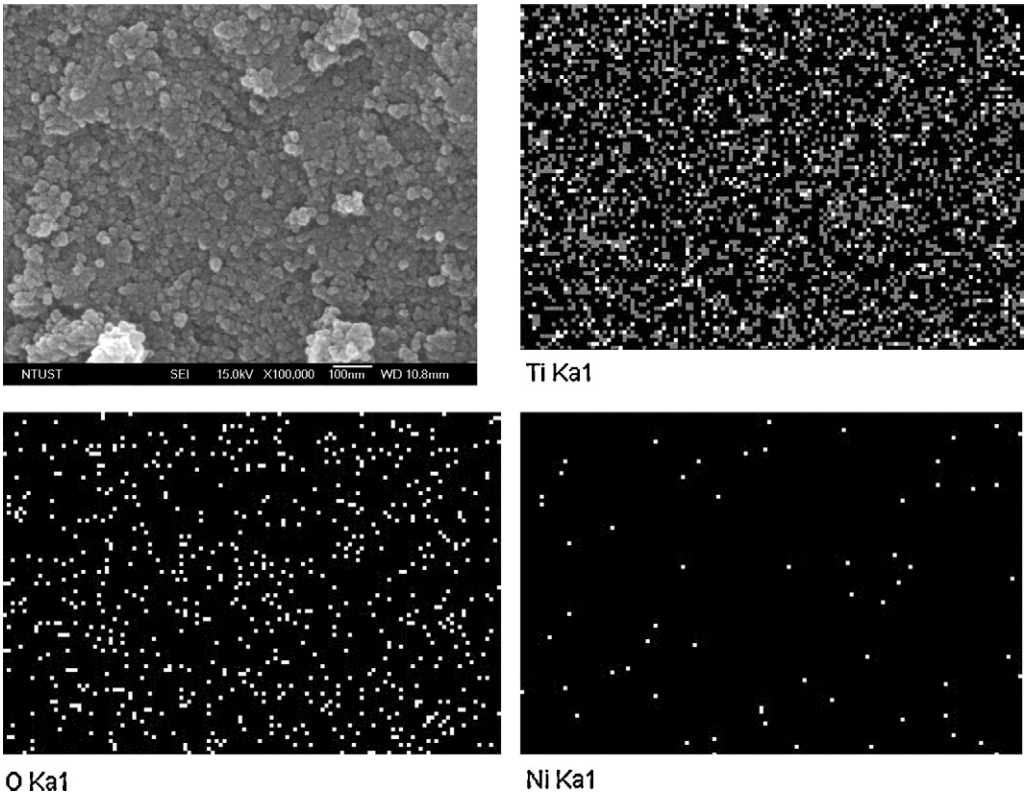

Fig. 4. SEM photograph and elemental mapping of NiO(0.1%)/TiO_2 coupled photocatalyst.

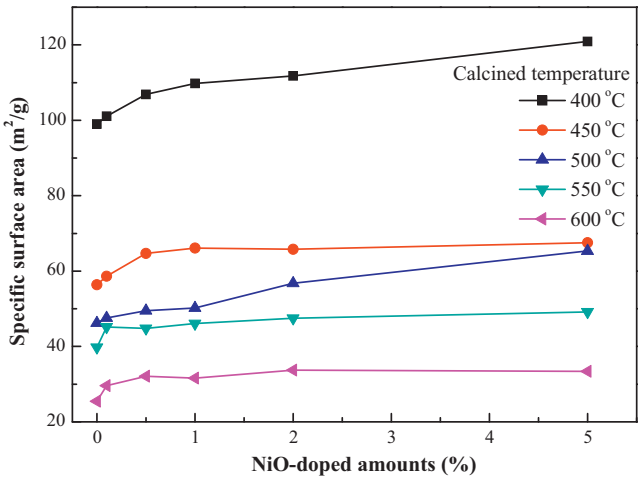

Fig. 5. Specific surface area of TiO_2 coupled with various dosages of NiO.

from anatase (1 0 1) to rutile (1 1 0). However, the crystalline phase of NiO could not be detected by XRD when the NiO(0.1%)/TiO_2 samples were calcined in the temperature range of 300–600 °C, possibly because the low content of NiO was uniformly dispersed, similar to the results observed by Wang et al. [13].

Examining the SEM images shown in Fig. 3 for NiO/TiO_2 samples calcined at temperatures between 400 and 600 °C, TiO_2 and NiO particles was hard to be distinguished from the SEM images because the shape and size of both particles was similar. The elemental mapping using 2D-EDX from SEM analysis was carried out on samples of the NiO/TiO_2 coupled photocatalysts. As shown in Fig. 4, the elemental mapping of titanium, oxygen and nickel in a sample of NiO(0.1%)/TiO_2 shows that the three element are uniformly distributed throughout the coupled catalyst. The uniform distribution of nickel dots was observed indicating the existence of NiO particle. The specific surface area of NiO/TiO_2 samples calcined at various temperatures is plotted as a function of doped NiO dosages as shown in Fig. 5. The specific surface area of NiO/TiO_2 particles was found to be decreased with increasing calcination temperature because of the aggregation of particles driven by heat-treatment. The decrease of surface area of NiO/TiO_2 particles would lead to the reduction of active sites and decrease the photocatalytic activity. Also shown in Fig. 5, the specific surface area of NiO/TiO_2 particles calcined at various temperatures was found to be slightly increased with increasing amount of NiO. It possibly could be attributed that the presence of NiO would hinder the aggregation of particles. Xia et al. [14] reported that the loading of lanthanum ions inhibited the growth of TiO_2 particles, and therefore increased the surface area of catalysts calcined at the same temperature.

XRD patterns of the prepared NiO/TiO_2 particles calcined at 500 °C are shown in Fig. 6(a). The results show that the diffraction peaks of NiO cannot be clearly found for the prepared NiO/TiO_2 particles containing less than 2% NiO. A weak diffraction peak at 2θ of 43.1° for NiO (2 0 0) plane was observed for NiO/TiO_2 particles containing 5% NiO. The intensities of diffraction peaks of anatase slightly decreased with increasing dosages of NiO. The calculated particle sizes of samples by Scherrer equation were 18.83, 16.17, 14.97, 14.11, 13.17 and 11.15 nm for NiO/TiO_2 particles containing 0, 0.1, 0.5, 1, 2 and 5% NiO, respectively. The decrease of particle sizes of NiO/TiO_2 containing higher dosage of NiO was attributed that the existence of NiO nanoparticles would hinder the aggregation of TiO_2 as mentioned above. As shown in Fig. 6(b), XRD patterns of NiO/TiO_2 calcined at 600 °C exhibits a diffraction peak at 2θ of 33° for $NiTiO_3$. The existence of $NiTiO_3$ might due to the fact that the calcination temperature of 600 °C was high enough for the reaction between NiO and TiO_2 to form $NiTiO_3$. Moreover, only anatase

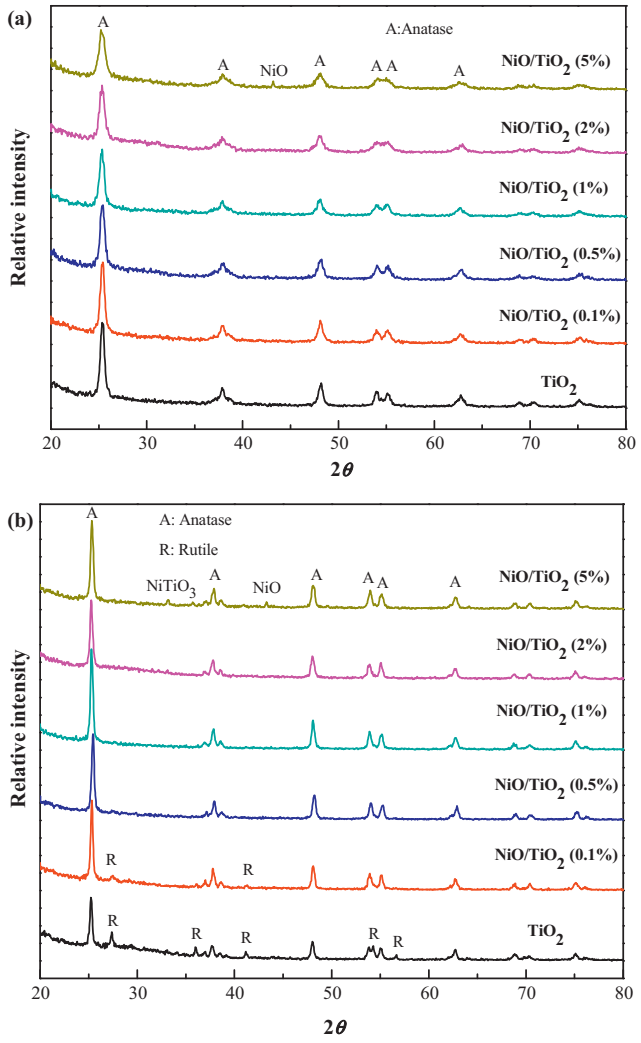

Fig. 6. XRD patterns of TiO_2 coupled with various dosages of NiO and calcined at (a) 500 and (b) 600 °C for 2 h.

was found in XRD patterns for NiO/TiO_2 containing NiO greater than 0.5%. The transformation temperature of TiO_2 from anatase to rutile was elevated significantly with increasing NiO dosage. Mohammadi and Fray [15] prepared NiO and TiO_2 composites by sol–gel method and revealed that phase transformation from anatase to rutile was hindered by the introduction of nickel, possibly because the presence of Ni^{2+} ions might stabilize the anatase phase.

Fig. 7 shows the UV–vis diffuse reflectance spectra of the NiO/TiO_2 containing various dosages of NiO. For pure TiO_2, the presence of strong absorption band near 350 nm indicates that the electrons were excited from valence band (O 2p states) to conduction band (Ti 3d states) [16]. The absorption edge of coupled photocatalysts was found to shift towards visible region with the presence of NiO. Moreover, the extended absorption edge to visible region reveals the good contact between NiO and TiO_2 in consequence of the inter-dispersion of the two oxides. In the contacting region, the composite conduction band mixed by Ti and Ni 3d states was essential to decrease the band gap energy between Ti 3d and O 2p states of Ti oxide [17]. Bokhimi et al. [18] also reported that the UV–vis diffuse reflectance spectra of CuO/TiO_2 exhibited extended absorption edge to visible region induced from the valence band of CuO to the conduction band of TiO_2 because of a good contact between CuO and TiO_2 crystals.

XPS full scan spectra of NiO(5%)/TiO_2 calcined at 500 °C for 2 h are shown in Fig. 8. The binding energies for Ti $2p_{3/2}$, O 1s, C 1s

Table 1
Composition (at.%) and binding energy (E_b) of TiO_2 doped with various dosages of NiO determined by XPS analyses.

Catalyst	Ti 2p		O 1s		C 1s		Ni 2p	
	at.%	E_b (eV)	at.%	E_b (eV)	at.%	E_b (eV)	at.%	E_b (eV)
0% (pure TiO_2)	24.31	458.84	60.70	530.27	15.00	284.59	–	–
0.1%	24.52	459.33	60.38	529.81	15.10	284.47	–	–
0.5%	24.23	459.16	59.17	529.89	16.47	284.55	0.13	853.74
1%	24.12	458.81	59.53	530.08	16.05	284.57	0.30	853.61
2%	23.46	458.84	60.64	529.91	15.18	284.58	0.72	853.90
5%	22.68	458.82	59.74	530.05	16.10	284.55	1.48	853.59

[a] at.% represents the atomic percent.

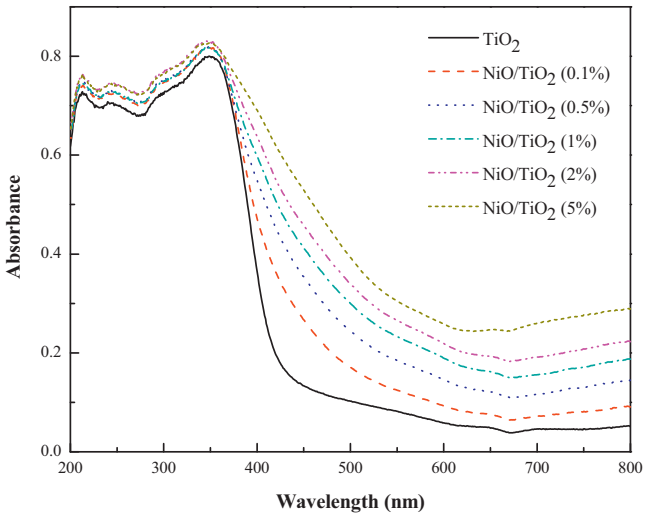

Fig. 7. UV–vis DRS patterns of TiO_2 coupled with various dosages of NiO and calcined at 500 °C for 2 h.

and Ni 2p were determined to be 458.8, 530.0, 284.7 and 853.8 eV, respectively, consistent with the data found in literature [19]. The high resolution scanning XPS spectra of Ni 2p shown in Fig. 9(a) designated two peaks at 853.8 and 871.7 eV, the peak intensity increased with increasing dosages of NiO. The binding energies of Ni, Ni^{2+} (NiO) and Ni^{3+} (Ni_2O_3) were reported to be 852.7–852.8, 853.5–854.3 and 855.8–857.3 eV, respectively [19]. Therefore, the peak of Ni $2p_{3/2}$ at 853.8 Ev, shown in Fig. 9(a) is assigned to NiO crystal.

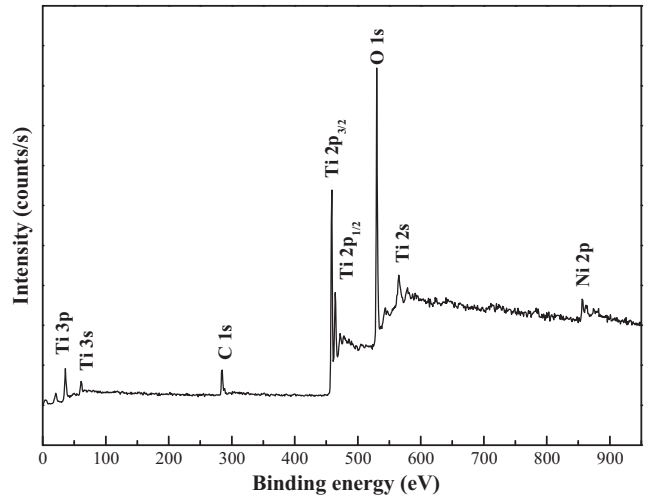

Fig. 8. XPS full scan spectra of NiO(5%)/TiO_2 calcined at 500 °C for 2 h.

XPS signals of Ti 2p were observed at 458.8 eV (Ti $2p_{3/2}$) and 464.6 eV (Ti $2p_{1/2}$), as shown in Fig. 9(b). The typical binding energy of Ti $2p_{3/2}$ peak was reported to be in the range of 458.5–459.7 eV [20]. The Ti $2p_{3/2}$ peaks of samples were narrow and symmetrical, with binding energy of 458.8 eV attributed to Ti^{4+}, indicating that Ni^{2+} was not incorporated into the lattice structure of TiO_2. Therefore, TiO_2 and NiO can be taken as independent existence in NiO/TiO_2 catalysts.

As illustrated in Fig. 9(c), the O 1s XPS spectrum of NiO(5%)/TiO_2 are wide and asymmetric, demonstrating that there are at least two forms of O binding state. The composition and binding energy of all elements on the surface of the catalysts are shown in Table 1. The O 1s XPS spectrum is resolved into two components by using Origin software with Gaussian rule. The results show the existence of two peaks at 529.9 and 531.4 eV matching the O lattice of titanium oxide (O 1s–Ti states, TiO_2) and the hydroxyl group in the water molecules adsorbed on the surface, respectively. The curve fitting results of O 1s are listed in Table 2. The O 1s peak of NiO was reported to be 529.3 eV [21], it is conjectured that this O 1s peak related to NiO may overlap with O 1s–Ti states.

Surface photovoltage spectroscopy (SPS) is a technique to characterize the illumination-induced changes in the surface voltage of semiconductive materials [22]. Fig. 10 revealed that the SPS responses obtained in this study for pure TiO_2, NiO(0.1%)/TiO_2 and NiO(5%)/TiO_2. The peak positions between 340 and 380 nm were attributed to the electrons excited from valence band (O_{2p}) to conduction band (Ti_{3d}) [23,24]. The peaks from 380 to 410 nm were assumed to be the responses of pure TiO_2 [23]. The SPS response of NiO(0.1%)/TiO_2 was higher than that of pure TiO_2 because the photogenerated electrons and holes can be efficiently separated by the p–n junction. The recombination of electron–hole pairs was therefore inhibited because the increases of surface photovoltage, comparable results were reported by Xin et al. [14] for Cu/TiO_2 photocatalysts. However, excessive loadings of 5% NiO reduced the SPS response possibly because NiO particles might serve as the recombination centers for electrons and holes.

The pH_{zpc} of TiO_2 photocatalysts doped with various NiO dosages are shown in Fig. 11. The pH_{zpc} values were found to be fairly constant for NiO/TiO_2 containing less than 1% of NiO. However, the pH_{zpc} were elevated for NiO/TiO_2 containing more

Table 2
Curve fitting result of high resolution XPS spectra for the O 1s region on the surface of TiO_2 doped with various dosages of NiO.

Catalyst	O 1s (Ti–O)		O 1s (–OH)	
	r_i (%)[a]	E_b (eV)	r_i (%)[a]	E_b (eV)
0% (pure TiO_2)	79.35	529.95	20.65	531.37
0.1%	81.79	529.76	18.21	531.08
0.5%	80.05	529.86	19.95	531.33
1%	81.81	530.03	18.19	531.51
2%	75.27	529.88	24.73	531.41
5%	75.97	529.95	24.03	531.45

[a] r_i (%) represents the ratio $A_i/\Sigma A_i$ (A_i is the area of each peak).

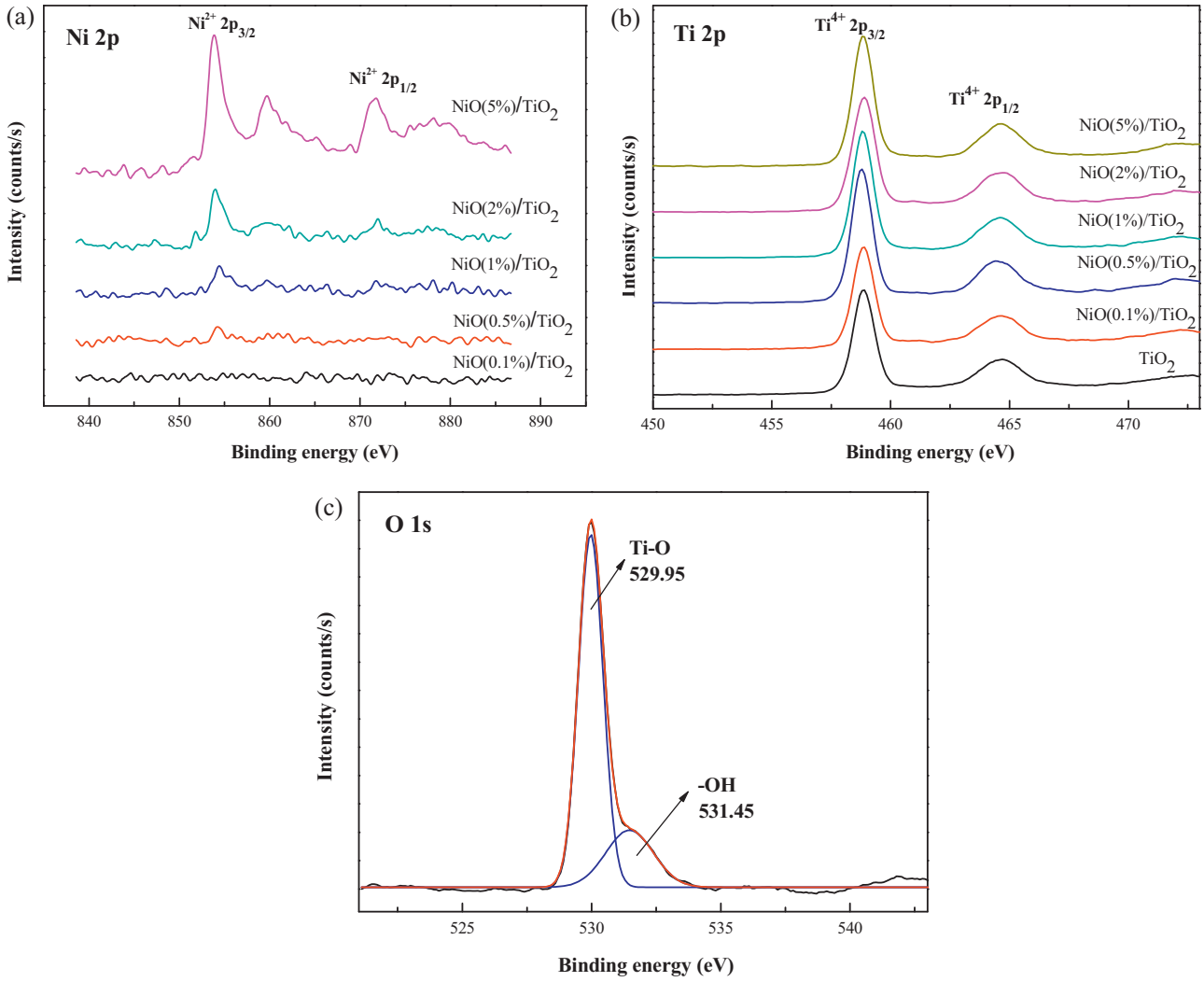

Fig. 9. High resolution XPS spectra of (a) Ni 2p and (b) Ti 2p region for the surface of TiO_2 coupled with various dosages of NiO, and peak fitted O 1s narrow scan spectrum of NiO(5%)/TiO_2.

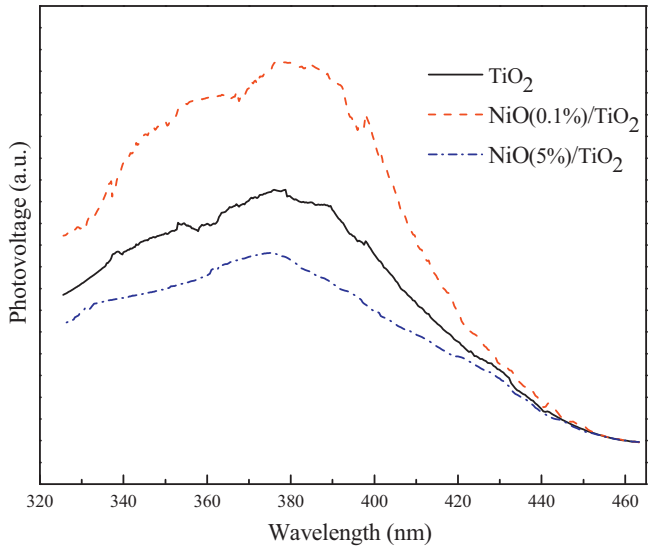

Fig. 10. SPS responses of TiO_2 coupled with various dosages of NiO.

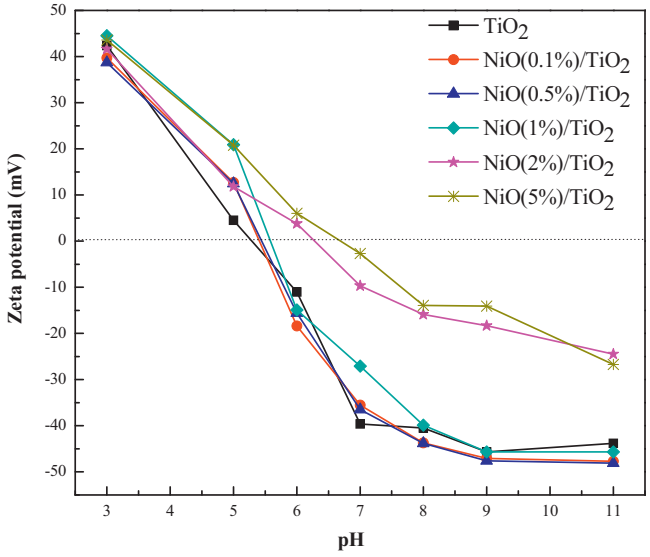

Fig. 11. Zeta potential of TiO_2 coupled with various dosages of NiO.

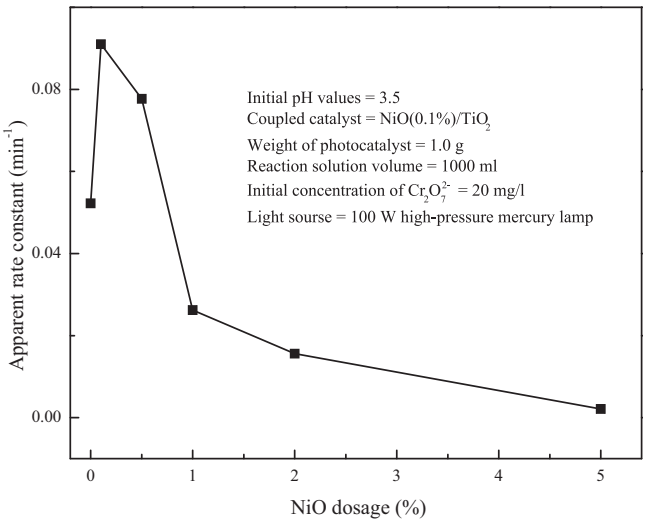

Fig. 12. Photocatalytic reduction of Cr(VI) in aqueous solutions using TiO_2 coupled with various dosages of NiO and calcined at 500 °C for 2 h.

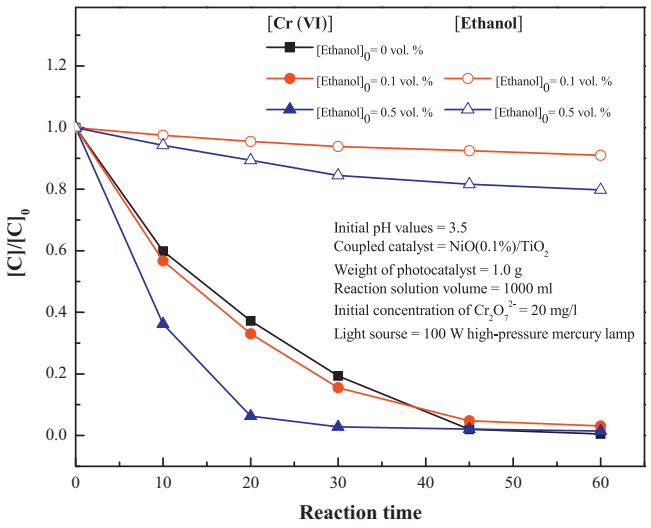

Fig. 14. Effect of ethanol on photocatalytic reduction of Cr(VI) in aqueous solutions using NiO/TiO_2.

than 2% NiO loading comparable observations were reported by Taylor et al. [25] and Pál et al. [26] for aluminum-doped TiO_2 and indium-doped ZnO, respectively. The surface of NiO/TiO_2 was positively-charged in aqueous solutions with pH less than pH_{zpc}, and offered a favorable condition to adsorb negatively charged particles and molecules.

Several researchers stated that NiO/TiO_2 exhibited higher activity for various photocatalytic reactions [11,27]. In this study, the photocatalytic activity of prepared NiO/TiO_2 was examined by carrying out the photocatalytic reduction of Cr(VI) in aqueous solutions. As shown in Fig. 12, the reduction of Cr(VI) were enhanced using the TiO_2 coupled with 0.1% and 0.5% NiO than that using pure TiO_2. The enhancements could be attributed that the presence of NiO develops a p–n junction to separate electron–hole pairs effectively. The schematic diagram of charge transfer of photogenerated electrons and holes under p–n junction mechanism for photocatalytic process was drawn as in Fig. 13. The inner electric field caused by p–n junction region could efficiently transfer the photogenerated holes into NiO, and then retard the recombination of

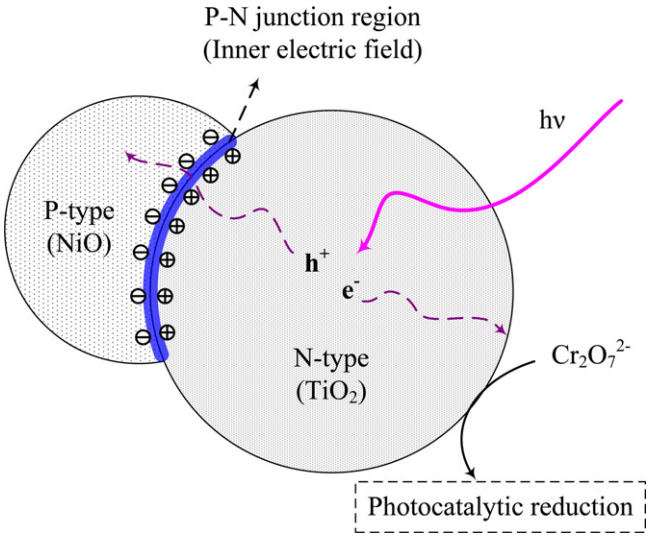

Fig. 13. Schematic diagram of charge transfer of photogenerated electrons and holes for photocatalytic process using NiO/TiO_2.

Table 3
Photocatalytic reduction of Cr(VI) in aqueous solutions using $NiO(0.1\%)/TiO_2$ calcined at various temperatures for 2 h.

Calcination temperature (°C)	Reaction rate constant (min^{-1})	R^2
400	0.044	0.968
450	0.0599	0.996
500	0.091	0.959
550	0.0136	0.937
600	0.0011	0.949

Reaction conditions: $C_{catalysts}$ = 1.0 g/L; $C_{Cr(VI)}$ = 20 mg/L; light source = 100 W high-pressure mercury lamp (365 nm); reaction solution volume = 1 L.

photogenerated electron–hole pairs. However, the photocatalytic activity was found to be decreased with increasing dosage of NiO for photocatalysts containing more than 1% NiO. The decrement of photocatalytic activity could be attributed to that the excessive NiO loadings would serve as the recombination centers for electrons and holes.

Photocatalytic reduction of Cr(VI) in aqueous solutions using $NiO(0.1\%)/TiO_2$ calcined at various temperatures are shown in Table 3. Experiments using $NiO(0.1\%)/TiO_2$ calcined at 500 °C exhibited maximum Cr(VI) reduction, because it was more crystallined than those calcined lower than 500 °C, and provided larger surface area than those calcined higher than 500 °C. In order to accelerate photocatalytic reductions, various organic compounds were added in aqueous solution to serve as hole scavenger [28–30]. In this study, various loadings of ethanol were added in the photocatalytic process, as shown in Fig. 14. The photocatalytic reduction of Cr(VI) was enhanced with increasing loading of ethanol for each NiO/TiO_2 photocatalyst coupled with various NiO dosages (not shown in figure). In the presence of 0.5 vol.% ethanol, more than 95% Cr(VI) was photocatalytically reduced within first 20 min of reaction time. The consumption of ethanol was in proportion to the enhancement of photocatalytic reduction of Cr(VI). The addition of ethanol used as a sacrificial agent efficiently depleted the photogenerated holes and significantly increased the photocatalytic reduction of Cr(VI).

4. Conclusions

From the characteristic analysis, coupling of NiO strongly affected the physical characterizations of the prepared coupled NiO/TiO_2 photocatalysts. The specific surface area of NiO/TiO_2

particles was found to be decreased with increasing calcination temperature because of the aggregation driven by heat-treatment. The slightly increased specific surface area of NiO/TiO_2 particles with increasing amount of NiO possibly could be attributed to the hindrance of aggregating particles by the presence of NiO. The extended absorption edge to visible region revealed the good contact between NiO and TiO_2. The photovoltage intensity of $NiO(0.1\%)/TiO_2$ was higher than that of pure TiO_2 because NiO captured the photogenerated holes while TiO_2 trapped the electrons by the p–n junction. In the photocatalytic activity of Cr(VI) reduction, experiments using $NiO(0.1\%)/TiO_2$ calcined at 500 °C exhibited favorable photocatalytic reduction of Cr(VI). The enhancements of photocatalytic reduction of NiO/TiO_2 could be attributed that the presence of NiO develops a p–n junction to separate electron–hole pairs effectively. The addition of ethanol improved the photocatalytic reduction of Cr(VI) because of the depletion of photogenerated holes by the consumption of ethanol.

Acknowledgements

This research was financially supported by Grant NSC 98-2221-E-011-020-MY3 from the National Science Council, Taiwan, Republic of China.

References

[1] Y. Ku, W.H. Lee, W. Wang, J. Chin. Inst. Environ. Eng. 13 (2003) 243–250.
[2] X. Chen, S.S. Mao, Chem. Rev. 107 (2007) 2891–2959.
[3] Y. Ku, I.L. Jung, Water Res. 35 (2001) 135–142.
[4] S. Chakrabarti, B. Chaudhuri, S. Bhattacharjee, A.K. Ray, B.K. Dutta, Chem. Eng. J. 153 (2009) 86–93.
[5] Chen, W. Zhao, W. Liu, S. Zhang, Appl. Surf. Sci. 255 (2008) 2478–2484.
[6] S. Wei, Y. Chen, Y. Ma, Z. Shao, J. Mol. Catal. A: Chem. 331 (2010) 112–116.
[7] Q. Wang, J. Shang, T. Zhu, F. Zhao, J. Mol. Catal. A: Chem. 335 (2011) 242–247.
[8] A. Kudo, K. Domen, K. Maruya, T. Onishi, Chem. Phys. Lett. 133 (1987) 517–519.
[9] D.W. Hwang, H.G. Kim, J.K. Kim, K.Y. Cha, Y.G. Kim, J.S. Lee, J. Catal. 193 (2000) 40–48.
[10] H. Kato, K. Asakura, A. Kudo, J. Am. Chem. Soc. 125 (2003) 3082–3089.
[11] T. Sreethawong, Y. Suzuki, S. Yoshikawa, Int. J. Hydrogen Energy 30 (2005) 1053–1062.
[12] R.C. Korošec, P. Bukovec, J. Therm. Anal. Calorim. 56 (1996) 587–596.
[13] J. Wang, L. Dong, Y. Hu, G. Zheng, Z. Hu, Y. Chen, J. Solid State Chem. 157 (2001) 274–282.
[14] H.L. Xia, H.S. Zhuang, D.C. Xiao, T. Zhang, J. Alloys Compd. 465 (2008) 328–332.
[15] M.R. Mohammadi, D.J. Fray, Solid State Sci. 12 (2010) 1629–1640.
[16] B.J. Morgan, G.W. Watson, Surf. Sci. 601 (2007) 5034–5041.
[17] J. Guo, W. Fu, H. Yang, Q. Yu, W. Zhao, X. Zhou, Y. Sui, J. Ding, Y. Li, S. Cheng, M. Li, J. Phys. D: Appl. Phys. 43 (2010) 24502–24508.
[18] X. Bokhimi, A. Morales, O. Novaro, Chem. Mater. 9 (1997) 2616–2620.
[19] J.F. Moulder, W.F. Stickle, P.E. Sobol, K.D. Bomben, Handbook of X-ray Photoelectron Spectroscopy, 2nd ed., Perkin-Elmer Corp, Minnesota, 1992.
[20] M. Yoshitake, A. Thananan, T. Aizawakia, K. Yoshihara, Surf. Interface Anal. 34 (2002) 698–702.
[21] M.C. Biesinger, B.P. Payne, L.W.M. Lau, A. Gerson, R.S.C. Smart, Surf. Interface Anal. 41 (2009) 324–332.
[22] L. Kronik, Y. Shapira, Surf. Sci. Rep. 37 (1999) 1–206.
[23] X.Z. Li, F.B. Li, C.L. Yang, W.K. Ge, J. Photochem. Photobiol. A 141 (2001) 209–217.
[24] L. Jing, X. Sun, W. Cai, Z. Xu, Y. Du, H. Fu, J. Phys. Chem. Solids 64 (2003) 615–623.
[25] M.L. Taylor, G.E. Morris, R.St.C. Samrt, J. Colloid Interface Sci. 262 (2003) 81–88.
[26] E. Pál, V. Hornok, A. Oszkó, I. Dékány, Colloids Surf. A 340 (2009) 1–9.
[27] Y.S. Chen, J.C. Crittenden, S. Hackney, L. Sutter, D.W. Hand, Environ. Sci. Technol. 39 (2005) 1201–1208.
[28] N.S. Foster, R.D. Noble, C.A. Koval, Environ. Sci. Technol. 27 (1993) 350–356.
[29] S. Wang, Z. Wang, Q. Zhuang, Appl. Catal. B 1 (1992) 257–270.
[30] M.R. Prairie, L.R. Evans, B.M. Stange, S.L. Martinez, Environ. Sci. Technol. 27 (1993) 1776–1782.